Low-pressure plasma-enhanced behavior of thermionic converters

Amir H. Khoshaman and Alireza Nojeh

Citation: J. Appl. Phys. **120**, 243302 (2016); doi: 10.1063/1.4972339
View online: http://dx.doi.org/10.1063/1.4972339
View Table of Contents: http://aip.scitation.org/toc/jap/120/24
Published by the American Institute of Physics

JOURNAL OF APPLIED PHYSICS **120**, 243302 (2016)

Low-pressure plasma-enhanced behavior of thermionic converters

Amir H. Khoshaman[a] and Alireza Nojeh[a]
Department of Electrical and Computer Engineering, University of British Columbia, Vancouver, British Columbia V6T 1Z4, Canada

(Received 7 November 2016; accepted 2 December 2016; published online 30 December 2016)

High-pressure plasmas have historically been used in thermionic energy converters both to reduce the electrode workfunctions and to mitigate the space-charge effect. The behavior of such devices has been studied extensively, but low-pressure thermionic converters are far less understood. Advances in nanotechnology, such as the possibility to intercalate nanomaterials-based electrodes with alkali metals in order to reduce workfunction, may alleviate the need for high gas pressures; low-pressure devices may thus play a significant role in future if they can address the space-charge problem. Here, we develop the physics of low-pressure thermionic converters by solving the Vlasov-Poisson system of equations self-consistently. We demonstrate that various possibilities arise due to intricate interactions between the spatially varying electron and ion concentrations, leading to phenomena such as plasma oscillations at higher ion fluxes. We show that even a relatively low ion flux density ($\sim 5 \times 10^{-4}$ times the flux density of electrons) reduces space-charge significantly and increases the electron current density by a factor of 7. We further extend the model by including electron and ion emission from both the cathode and anode electrodes. *Published by AIP Publishing*. [http://dx.doi.org/10.1063/1.4972339]

INTRODUCTION

A thermionic energy converter (TEC), in its simplest form, comprises a hot electrode (emitter or cathode) separated by a vacuum or plasma gap from another electrode (collector or anode). The circuit is closed through an external load. This device can be used to directly convert heat to electricity. TECs have been studied for over a century, with significant interest starting in the 1950s. Two main factors that have hampered the progress of these devices are the space-charge effect, i.e., a motive peak in the inter-electrode region of the device due to the presence of electrons, and the difficulty in finding materials with very low workfunction and yet favorable thermal and mechanical properties. There has been a new wave of interest in this field in recent years due to the availability of new fabrication technologies and nanomaterials, which may help overcome these issues.[1–5] An overview of some of the advances in thermionic conversion enabled by nanotechnology is given in Ref. 6.

Historically, the introduction of ions in the inter-electrode region has been the most popular method of overcoming the above-mentioned challenges. The positively charged ions neutralize the negative space-charge of the electrons and also reduce the workfunction of the emitter and collector by being adsorbed on their surfaces. However, in order to deposit on the emitter surface, a high concentration of neutral atoms is required due to the high temperature of the emitter. This is the basis of the operation of high-pressure vapor diodes. On the other hand, the presence of a high concentration of neutral atoms in the inter-electrode region causes scattering of the electrons and results in significant reduction of the electron current.[7] These high-pressure diodes have been studied using phenomenological models or magnetohydrodynamics equations.[8,9]

For typical operating conditions of a TEC (e.g., a potassium reservoir temperature of 700 K, leading to a vapor pressure of $\sim 10^3$ Pa (Ref. 10)), the mean free path between the charged particles (ions and electrons) and the neutral atoms is on the order of $\sim 50\,\mu$m. The electron concentration in TECs is typically several orders of magnitude less than the concentration of the neutral atoms under these conditions; therefore, a low-pressure plasma model is required to analyze this wide regime if the inter-electrode distance (d) is on the order of $\sim 100\,\mu$m for the aforementioned temperature.

The physics of high-pressure TECs has been studied extensively in the past, but the models developed are applicable only when the gas density is high. The phenomenological model of high-pressure TECs relies on solving drift and diffusion equations, which assume collisions with neutral particles. On the other hand, magnetohydrodynamic equations are truncated at some level (since the moments of the Boltzmann equation are solved for, rather than the transport equation itself[11]) and the diffusive (random walk) features of the movement of neutral atoms are introduced. Therefore, different sets of equations apply to the operation of TECs in low- and high-pressure plasma cases.

Future devices may take advantage of nanostructuring to create low-workfunction electrodes and only require space-charge reduction, for which a low-pressure plasma is sufficient in some cases as shown below. A few works in the 1960s and 1970s have dealt with low-pressure TECs.[9,12,13] These works either rely on finding analytical or qualitative solutions to the transport equation, which severely limits their applicability, or provide numerical solutions only in special cases. The ability to quantitatively treat the entire range of possibilities in low-

[a]Authors to whom correspondence should be addressed. Electronic addresses: akhosham@ece.ubc.ca and anojeh@ece.ubc.ca

pressure TECs is imperative for engineering new devices. Our model is based on numerical, self-consistent solutions to the Vlasov-Poisson system of equations and, by including the momentum gaps and using asymptotic expansions of the ill-behaving mathematical functions, addresses this crucial need.

Our approach allows us to solve the Vlasov equation even in cases where an analytical solution does not exist or becomes intractable (i.e., in the presence of several peaks in the motive). We propose an algorithm to calculate the charge carrier densities and motives under any condition that may arise in the operation of low-pressure TECs. We include all the electron-electron, electron-ion, and ion-ion interactions in the Poisson equation in a mean-field fashion and introduce the resulting motive as a force term in the Vlasov equation. We further demonstrate that under certain initial conditions, momentum gaps arise in the phase-space of the electrons and ions.

In our previous work, we demonstrated that, in a vacuum TEC comprising a biased grid between its emitter and collector, the electron phase-space can exhibit momentum gaps.[14] This happens when two motive peaks exist in the inter-electrode region such that the peak closer to the emitter is shorter than the peak closer to the collector: reflection of electrons from the first peak prevents those with low energy from entering the motive well between the two peaks. The inclusion of the resulting momentum gaps in the model was crucial in the investigation of the effect of the grid in mitigating the space-charge effect. In this work, we extend our self-consistent approach to include the presence of ions in the inter-electrode region. Here, in contrast to the case of having a grid in a predefined position, the positive charge distribution is not fixed. As a result, the device containing ions is more complex in terms of both modeling and the phenomena that can arise, as explained below.

We illustrate that, depending on the flux of the ions, different scenarios develop. At sufficiently low ion fluxes, the motive barrier is lowered, but the overall shape of the motive remains similar to the case where no ions are present. However, at higher ion fluxes, plasma oscillations appear and the motive is significantly altered. We finally extend the model to include electron and ion emission from both electrodes.

One of the main features of the proposed model is that our numerical and self-consistent approach to the Vlasov-Poisson equations can fully capture the physics of the system as it does not rely on finding analytical solutions that exist only in certain ranges of operation.[7,15] Moreover, our method provides salient advantages in terms of accuracy (lack of splicing errors[16,17] and making use of asymptotic expansion of the ill-behaving functions) and extendability (it can be applied in the presence of back-emission). This work also serves as a framework for further studies including three-dimensional analysis, which may become significant in nanomaterials-based TECs,[18] and time-dependent analysis, where analytical solutions do not exist.

THEORY

Depending on the concentrations of the electrons and ions, a variety of different motive profiles arise in the inter-electrode region. The motives differ in the number of peaks and valleys, and the relative heights of the different peaks. It is assumed that ions have a unit positive charge and therefore the motive that they experience is the negative of the electron motive. The motives start at the point outside the emitter ($x = 0$) and end at the point outside the collector ($x = d$, where d is the inter-electrode distance). Two special cases of motive profiles with 3 valleys and 2 peaks in the inter-electrode region are depicted in Fig. 1. Such motive profiles can arise for both electrons and ions depending on their concentrations.

We will describe the velocity distribution of the species (electrons or ions) in these cases for the purposes of illustration, and then provide a general algorithm applicable to an arbitrary motive profile. For points 3–4 and 11–12 in the motive on the left, the velocity distribution functions are the same as those of regular TECs and have been described before.[16] These distribution functions are

$$f_\sigma(x,v) = 2\,n_\sigma(x_M)\left(\frac{m_\sigma}{2\pi k_B T_E}\right)^{\frac{3}{2}} \exp\left(\frac{\psi_{M,\sigma} - \psi_\sigma(x)}{k_B T_E} - \frac{m_\sigma v^2}{2 k_B T_E}\right) \times \Theta(v_x \pm v_{x,min}), \quad (1)$$

where $\sigma \in \{e, i\}$, with e and i representing electrons and ions, respectively. $n_\sigma(x_M)$ is the concentration of species σ at the point of maximum motive, $\psi_{M,\sigma}$. m_σ is the mass of species σ, T_E is the emitter's temperature, k_B is the Boltzmann constant, x is the direction of propagation, v is the speed, and v_x is the velocity along the x direction. Also, $\psi_{M,i} = -\psi_{M,e}$, and $v_{x,min}$ represents the minimum permissible velocity of the charge carrier at position x, and we have $v_{x,min} = \left(2\frac{\psi_{M,\sigma} - \psi_\sigma(x)}{m_\sigma}\right)^{\frac{1}{2}}$. Θ is the unit step function, and the positive sign in its argument is for $x \le x_M$ (since negative velocities are permissible) and the negative sign for $x > x_M$.[7] In order to obtain these equations, the one-dimensional Vlasov equation is solved assuming that the electrons and ions adopt a hemi-Maxwellian distribution at the point of their maximum motive (different points for electrons and ions).

However, when the charge carriers are in regions 1–3 and 4–11, a gap arises in their velocity distribution function due to their reflection from the local maxima:

$$f_\sigma(x,v) = 2\,n_\sigma(x_M)\left(\frac{m_\sigma}{2\pi k_B T_E}\right)^{\frac{3}{2}} \exp\left(\frac{\psi_{M,\sigma} - \psi_\sigma(x)}{k_B T_E} - \frac{m_\sigma v^2}{2 k_B T_E}\right) \times \{\Theta(v_x - v_2) + \Theta(v_x + v_1) - \Theta(v_x + v_2)\}, \quad (2)$$

where $v_2 = \left(2\frac{\psi_{M,l,\sigma} - \psi_\sigma(x)}{m_\sigma}\right)^{\frac{1}{2}}$ and $v_1 = \left(2\frac{\psi_{M,\sigma} - \psi_\sigma(x)}{m_\sigma}\right)^{\frac{1}{2}}$. $\psi_{M,l,\sigma}$ is the local minimum (including the boundary points) and, in region 1–3, it is the motive of the emitter, i.e., $\psi(0) = 0$, whereas in region 4–11, it is equal to ψ_4. Therefore, for the velocity distributions at the top of Fig. 1, the local motive maxima used to calculate velocities v_2 and v_3 are at points 1 and 4, respectively. These distribution functions can be obtained based on the arguments that we made in Ref. 14 to analyze the electron dynamics in the presence of a grid. Briefly, since charge carriers are assumed to originate from one electrode and travel to the other, in each well only

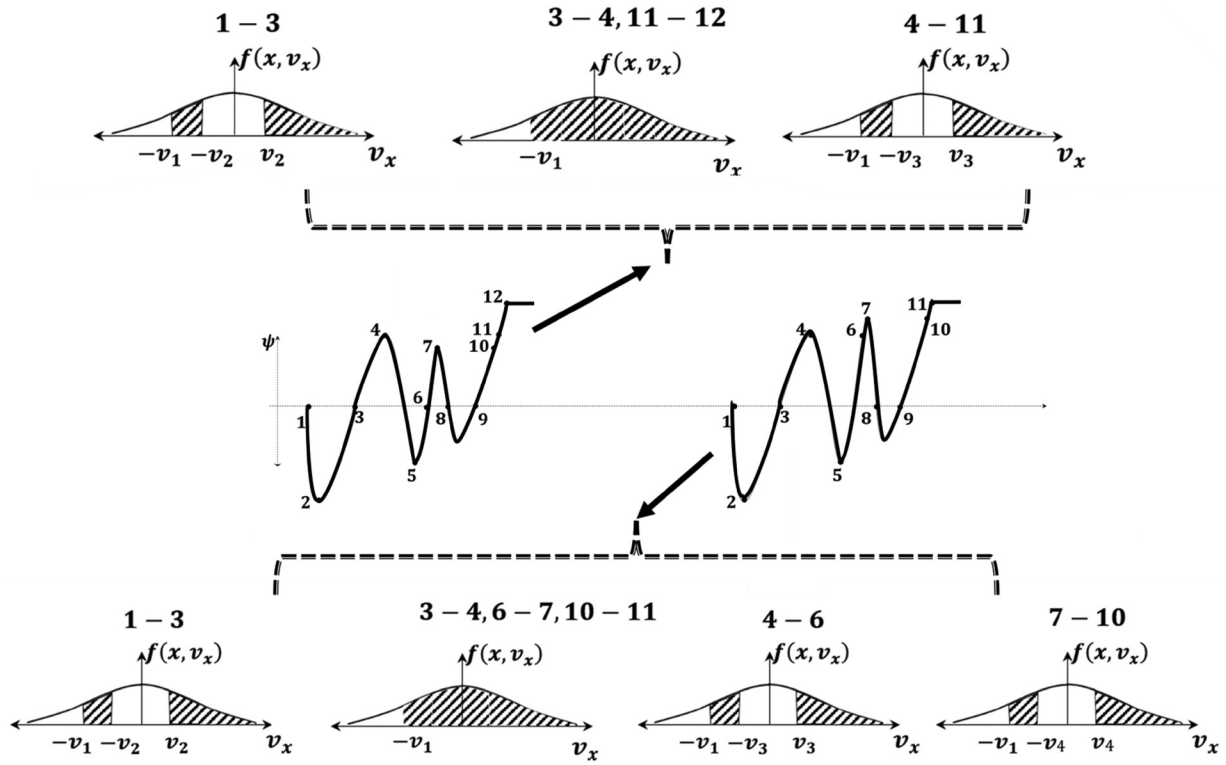

FIG. 1. The motive profile and the resulting distribution functions for electrons in two special cases where the number of valleys and peaks is 3 or less (the motive profile for positive ions is the negative of that for electrons). ψ is the motive; $f(x, v_x)$ is the velocity distribution function. v_x represents the velocity along the direction of propagation (x). Point 1 corresponds to the point just outside the emitter and the last point (11 or 12) represents the point just outside the collector. In the motive on the left, three regions with different velocity distribution functions exist, and there are two regions with two different momentum gaps. For the motive on the right, there are four distinct regions and three different momentum gaps. These motive profiles result from the combined effects of both electrons and ions. For the velocity distributions at the top, the local motive maxima that determine velocities v_2 and v_3 are at points 1 and 4, respectively, whereas for the velocity distributions at the bottom, the local motive maxima that determine velocities v_2, v_3, and v_4 are at points 1, 4, and 7, respectively.

electrons with initial kinetic energies higher than all the preceding peaks are present, since otherwise they would not be able to reach that region and would be reflected back. In contrast to the situation with a grid, in the case of the low-pressure plasma device, momentum gaps appear in multiple regions of space. For instance, for the motive on the right hand side of Fig. 1, three regions with distinct momentum gaps arise. These regions are distinguished by having different values of maximum local motives. For the velocity distributions at the bottom of Fig. 1, the local motive maxima used to calculate velocities v_2, v_3, and v_4 are at points 1, 4, and 7, respectively.

Although in Fig. 1 the number of peaks and valleys is less than 4, Eqs. (1) and (2) can be modified to be applicable to any number of peaks and valleys. Assume that the peaks in the motive are numbered from 1 to n_p, where n_p is the total number of peaks. At an arbitrary point x, the distribution function is determined by the positive sign in the argument of Eq. (1) (electrons traveling unidirectionally) if x lies on the right hand side of peak n_M, where n_M is the index for the peak with the highest motive. The distribution function is determined by the negative sign in the argument of Eq. (1) for all points lying to the left hand side of the first peak, n_1, or at points between the peaks n_i and n_j ($j > i$) where the motive is higher than the motive at peak number n_i and lower than the motive at peak number n_j. At all other points x, the distribution is determined by Eq. (2) with different values of $n_\sigma(x_M)$, $\psi_{M,l,\sigma}$, and $\psi_{M,\sigma}$ determined by the highest peak prior to (to the left of) point x.

The resulting electron distributions are integrated and inserted into the Poisson equation:

$$\frac{d^2\psi(x)}{dx^2} = -\frac{e^2}{\epsilon_0}(n_e(x) - n_i(x)). \tag{3}$$

If the species' distribution is determined by Eq. (1), the resulting electron concentration is

$$n_\sigma(x) = n_\sigma(x_M)\exp(\gamma)(1 \pm \mathrm{erf}\,\gamma^{1/2}), \tag{4}$$

where $\gamma \equiv \frac{1}{k_B T_E}\left(\psi_{M,\sigma} - \psi_\sigma(x)\right)$. On the other hand, integration of Eq. (2) results in

$$n_\sigma(x) = n_\sigma(x_M)\exp(\gamma)(1 - 2\,\mathrm{erf}\,\gamma_l^{1/2} + \mathrm{erf}\,\gamma^{1/2}), \tag{5}$$

where $\gamma_l \equiv \frac{1}{k_B T_E}\left(\psi_{M,l,\sigma} - \psi_\sigma(x)\right)$. At high values of γ and γ_l, where the error functions approach 1, their asymptotic expansions are used to circumvent the numerical errors (by using 6 terms in the expansion, mean errors of less than 10^{-4}% are reached).[14] The Poisson equation and the electron densities resulting from the Vlasov equation (Eqs. (3)–(5)) are solved recursively based on the method that we have proposed before.[15] Briefly, Eq. (3) is solved using the finite-difference method with the inter-electrode region divided into 10000 points. (Further refinement of the spatial mesh

results in mean variations of less than $\sim 10^{-5}$ % in the calculated motive.) At each stage, the electron densities are updated based on the integration of the velocity distribution functions (Eqs. (4) and (5)). The Richardson-Dushman equation[15] and the incident flux of the ions (calculated from the Saha-Langmuir equation (Eq. (6) below)) are used to calculate $n_e(x_M)$ and $n_i(x_M)$, respectively. The Saha-Langmuir equation can be written as

$$J_{sat,i} = \frac{eP}{(2\pi m_i k_B T_R)^{1/2}\left\{1 + 2\exp\left[\frac{E_i - \phi}{k_B T}\right]\right\}}, \tag{6}$$

where P is the vapor pressure of the alkali metal, T_R is the alkali metal reservoir temperature, E_i is the ionization energy of the alkali metal, and ϕ and T are the workfunction and the temperature, respectively, of the emitter or collector.[7,8]

RESULTS AND DISCUSSION

The ion flux densities used in the following calculations are evaluated based on realistic experimental alkali metal vapor pressures.[10] These values are converted into ion flux densities using Eq. (6). When the flux of the ions is sufficiently low, their influence on the behavior of the TEC is the reduction of space-charge, with no dramatic changes in the motive profile. For instance, when the saturation flux density of the ions, $J_{sat,i}$, is 10^{-4} times smaller than that of the electrons, $J_{sat,e}$ (given by the Richardson-Dushman equation), i.e., when $\beta \equiv \frac{J_{sat,i}}{J_{sat,e}} = 10^{-4}$, the maximum motive is reduced by 0.05 eV (Fig. 2(a)) in a TEC with the parameters given in the caption of Fig. 2.

For each of the cases studied in Fig. 2, a mixing ratio parameter, α (Ref. 15) is defined which determines the weight by which the motive is updated at each iteration. Each iteration yields the current density obtained from the solution to the Vlasov equation, i.e., the steady state current density obtained if the motive is frozen at its given value. The motive and carrier densities in Fig. 2 all converge and, therefore, the system is stable and reaches a DC steady-state with no plasma oscillations. Fig. 2(b) shows the electron concentration as a function of distance. It can be observed that in the presence of ions, a higher number of electrons are allowed in the inter-electrode region, although the overall motive is reduced in Fig. 2(a). Moreover, the electron concentration becomes smaller as the electrons propagate towards the collector, as one would expect in regular TECs as well. The ion concentration, on the other hand, has a minimum value somewhere in the inter-electrode region and has its highest values closer to the electrodes (Fig. 2(c)) when $\beta = 10^{-4}$.

The situation is different when $\beta = 5 \times 10^{-4}$. In this case, the ion concentration (Fig. 2(c)) is high enough to induce negative motives at some points (Fig. 2(a)). The electron concentration is nonetheless a mostly decreasing function of distance, since they face only one barrier on their way to the collector (Fig. 2(a)). Moreover, since the current density plateaus at higher iteration numbers, the system is stable and a DC solution to this plasma-enhanced TEC is obtained. According to Fig. 2(a), the maximum motive is reduced by 0.24 eV compared to the case where no ions are present, corresponding to a 7–fold increase in output current density.

If the saturation flux density of the ion emission is increased further, plasma oscillations occur and the system will not have a stable DC behavior in the steady state. This happens only if the maxima of the electron and ion densities both occur at some points in the inter-electrode region, rather than the points just outside the emitter and collector. In such cases, the electrons tend to travel from the point of their

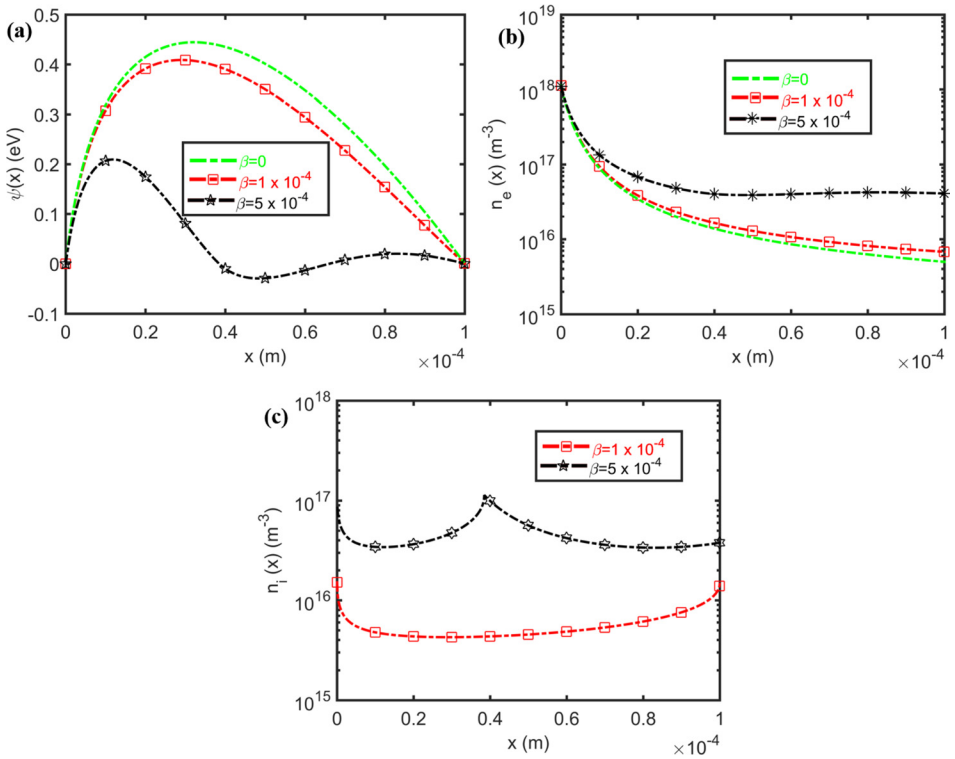

FIG. 2. The characteristics of a TEC in the presence of ions for $\beta = 0$, 10^{-4} and 5×10^{-4}. The workfunctions of the emitter and the collector are $\phi_E = \phi_C = 2.5$ eV, the emitter's temperature is $T_E = 1500$ K, and the inter-electrode distance is $d = 100\,\mu$m. The resulting (a) motive, $\psi(x)$, (b) electron concentration, $n_e(x)$, and (c) ion concentration, $n_i(x)$, are plotted. $\beta = 0$ represents the absence of ions.

highest concentration to a position with the highest ion concentration. Therefore, a static steady state can never be attained and the electron and ion densities, as well as the motive, change cyclically and in response to each other. The only conceivable exception is when the point with maximum electron concentration coincides with the point with maximum ion concentration, which cannot occur based on the distribution functions described by Eqs. (1)–(2). In terms of motive, this phenomenon arises when momentum gaps are present in the phase-space of the propagation of both the electrons and the ions, so that there is at least one region for each species where the velocity distribution function follows Eq. (2). In the TEC described in Fig. 2, when $\beta = 10^{-4}$, no momentum gap is present in the phase-space of either electrons or ions. In contrast, when $\beta = 5 \times 10^{-4}$, momentum gaps exist for the transport of ions, but not electrons.

Fig. 3 portrays the characteristics of a TEC with a higher value of ion saturation flux density ($\beta = 10^{-3}$). Fig. 3(a) depicts the evolution of the current density as a function of the iteration number. The values of α are typically chosen to be small in the beginning ($\alpha = 10^{-3}$) and then gradually increased to $\alpha = 0.1$ when the solutions to the Poisson and Vlasov equation become more consistent as the initial numerical instabilities have abated. The values of α are reduced again to $\alpha = 10^{-3}$ at higher stages.

As observed from Fig. 3(a), a DC steady state current density cannot be obtained as the current oscillates between several values. According to Figs. 3(b) and 3(c), both electrons and ions have their maximum concentrations in the inter-electrode region. The motive profile at $n = 2763$ corresponds to the case where the electrons do not have a momentum gap in their phase-space, whereas the ions, seeing the negative of the motive experienced by the electrons, do indeed have a momentum gap and will have their maximum concentration in the inter-electrode region. At $n = 3434$, a new peak emerges and, beyond this iteration, the electrons will adopt a momentum gap. $n = 3878$ is the mid-point between the two more extreme cases of $n = 1294$ and $n = 1300$. This process repeats itself, leading to oscillations in the charge carrier densities and the motive.

Based on Fig. 3(a), a common solution to the Poisson and time-independent Vlasov equations does not exist; therefore, a DC steady state cannot be attained for this value of ion flux density. The only possibility is that a time-independent solution does not exist and thus the system will have plasma oscillations. A time-dependent solution is not within the scope of this work. Such cases are extremely rare in low-pressure plasma TECs. For instance, to obtain the ion flux in Fig. 3, by using the potassium vapor pressure data[10] and the Saha-Langmuir equation,[8] a potassium reservoir temperature of 870 K is required. This corresponds to a neutral potassium pressure of ~ 13 kPa. The mean free path for the electrons and the gas molecules under such conditions can be estimated to be $\sim 70\,\mu$m which is already smaller than the inter-electrode distance (100 μm) and thus detrimental to device operation. Therefore, such cases are rarely subsumed within the operational regime of low-pressure plasmas. Nonetheless, an estimate for one of the time scales

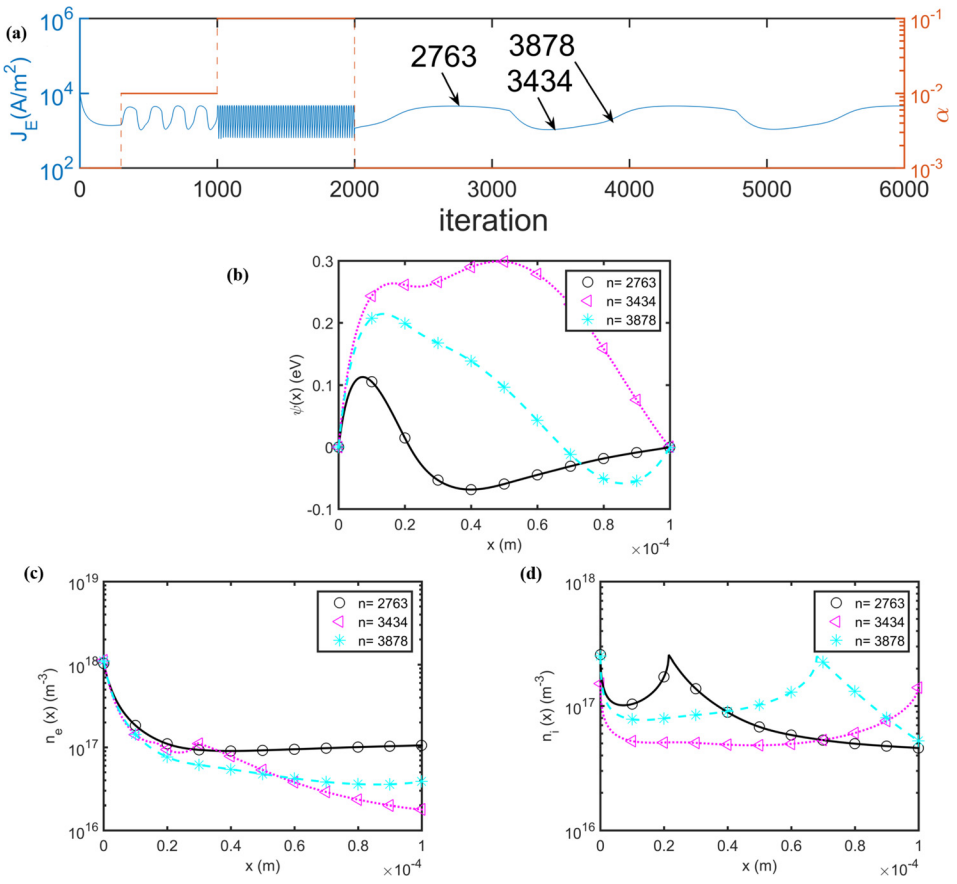

FIG. 3. The characteristics of a TEC with the same parameters as those of Fig. 2 but in the presence of ions with a flux density 1×10^{-3} times that of the electrons. These parameters lead to oscillations in the output characteristics of this TEC. Evolutions (in iteration number) of the (a) current density from the emitter, J_E, (b) motive, $\psi(x)$, (c) electron concentration, $n_e(x)$, and (d) ion concentration, $n_i(x)$, are plotted. The values of α are depicted on the right axis in (a).

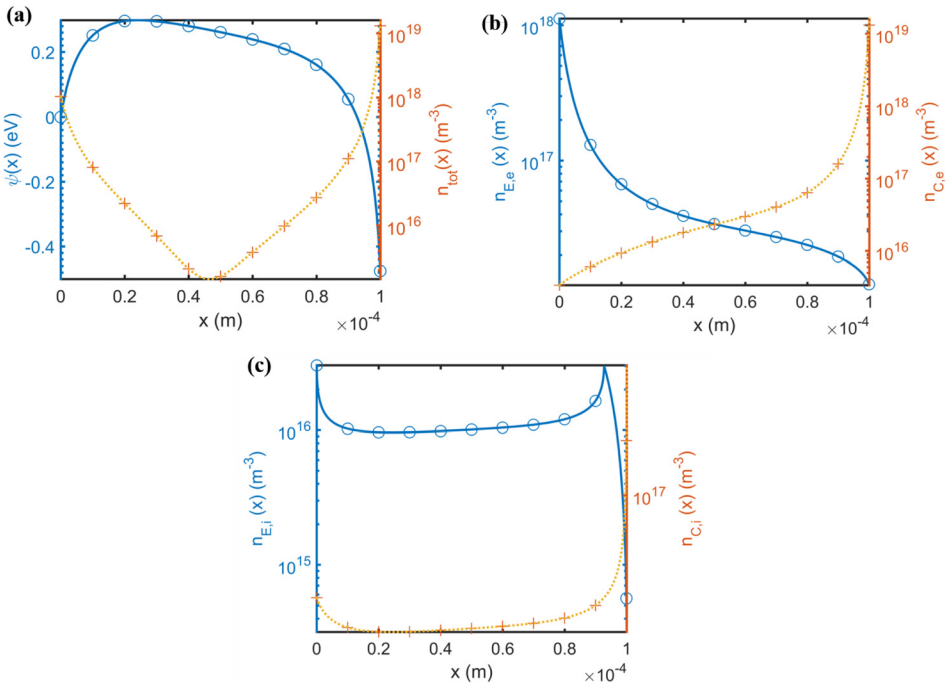

FIG. 4. The motive and carrier densities of a TEC with $\phi_E = 2.5\,\text{eV}$, $\phi_C = 2.0\,\text{eV}$, $T_E = 1500\,\text{K}$, $T_C = 1300\,\text{K}$, and $d = 100\,\mu\text{m}$. The ratio of the ion to electron flux densities is set equal to 10^{-4} for both the collector and the emitter. Spatial distributions of (a) the motive and total charge carrier concentration $n_{tot} \equiv |n_{E,e}(x) + n_{C,e}(x) - n_{E,i}(x) - n_{C,i}(x)|$; (b) the electron concentrations resulting from the emitter, $n_{E,e}(x)$, and the collector, $n_{C,e}(x)$; and (c) the ion concentrations resulting from the emitter, $n_{E,i}(x)$, and the collector, $n_{C,i}(x)$.

involved in the system may be obtained by noting that the velocity of the ions is on average several hundred times smaller than the velocity of the electrons. For instance, the average velocity of potassium ions is ~270 times smaller than that of the electrons. Therefore, this time scale is determined by the slower moving ingredients, i.e., the ions, and can be estimated to be $\sim 2d\left(\frac{m_a}{e\,\psi_M}\right)^{1/2} = 700\,\text{ps}$. This time scale is 2 orders of magnitude larger than the natural plasma oscillation period due to the ion concentration.

Considering that it is possible to create devices with very small inter-electrode distances using micro/nanofabrication, including the back-emission will be crucial in analyzing novel thermionic devices. Our model can be extended to include more general cases where back-emission of the ions and electrons from the collector is not negligible. Fig. 4 shows such a case for a TEC with the parameters provided in the figure caption. The same strategy as before was applied to calculate the output characteristics. The charge density inserted into the Poisson equation was calculated as the sum of all contributions, i.e., the electron concentration from the emitter, $n_{E,e}(x)$, the ion concentration from the emitter, $n_{E,i}(x)$, the electron concentration from the collector, $n_{C,e}(x)$, and the ion concentration from the collector, $n_{C,i}(x)$. Each one of these was calculated by integrating the corresponding velocity distribution function over the possible ranges of velocities. As observed from Fig. 4, the concentrations of electrons and ions arising from the emitter and collector are decreasing functions of distance, except when a momentum gap exists in the inter-electrode region; for the parameters studied in Fig. 4, a momentum gap arises in the phase-space of the ions that originate from the surface of the emitter (Fig. 4(c)).

The proposed method enables the calculation of the current density-voltage (J–V_{ap}) characteristics of the device under various operating conditions. Fig. 5 represents such characteristics with the parameters specified in Fig. 4, as a function of voltage difference between the collector and the emitter, V_{ap}. ψ_M represents the maximum motive and J_{tot} is the total current density from the emitter to the collector. As it can be observed from this figure, the overall effect of the introduction of ions is the reduction of space-charge. At small biases, the total current in the presence of ions is about 10 times larger than in the case where ions are absent.

SUMMARY

In summary, the physics of the operation of TECs in low-pressure plasmas was developed. It was observed that, depending on the ratio of the flux density of the ions to that of the electrons, a wide array of motive profiles arises. When this ratio is small, the effect of the ions is the reduction of the space-charge. However, as this ratio is enhanced, plasma oscillations occur. We also demonstrated the extendability of

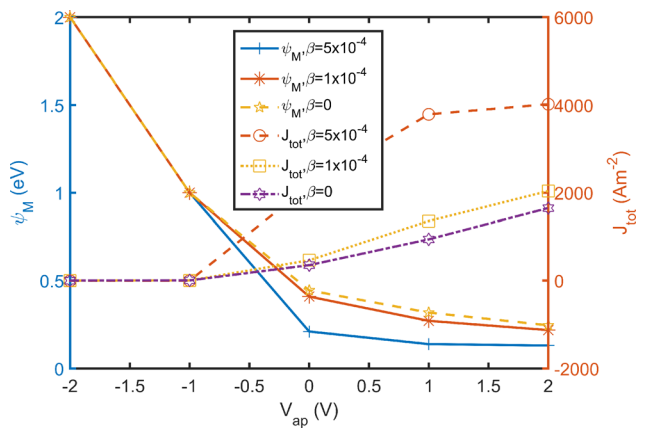

FIG. 5. The current density-voltage (V_{ap}) characteristics of the TEC with the parameters specified in Fig. 2. $\beta = 0$ corresponds to the case where no ions are present. ψ_M represents the maximum motive and J_{tot} is the total current density from the emitter to the collector.

the model by including electron and ion emissions from both the emitter and the collector.

ACKNOWLEDGMENTS

Financial support was provided by the Natural Sciences and Engineering Research Council of Canada (SPG-P 478867) and the Peter Wall Institute for Advanced Studies. Amir H. Khoshaman also thanks the University of British Columbia for additional support.

[1]T. L. Westover, A. D. Franklin, B. A. Cola, T. S. Fisher, and R. G. Reifenberger, "Photo- and thermionic emission from potassium-intercalated carbon nanotube arrays," J. Vac. Sci. Technol. B Microelectron. Nanometer Struct. **28**(2), 423–434 (2010).
[2]V. S. Robinson, T. S. Fisher, J. A. Michel, and C. M. Lukehart, "Work function reduction of graphitic nanofibers by potassium intercalation," Appl. Phys. Lett. **87**(6), 61501 (2005).
[3]A. H. Khoshaman, H. D. E. Fan, A. T. Koch, N. H. Leung, and A. Nojeh, "Localized light induced thermionic emission from intercalated carbon nanotube forests," in *27th International Vacuum Nanoelectronics Conference (IVNC)* (2014), pp. 59–60.
[4]S. Meir, C. Stephanos, T. H. Geballe, and J. Mannhart, "Highly-efficient thermoelectronic conversion of solar energy and heat into electricpower," J. Renewable Sustainable Energy **5**(4), 43127 (2013).
[5]J. R. Smith, G. L. Bilbro, and R. J. Nemanich, "Considerations for a high-performance thermionic energy conversion device based on a negative electron affinity emitter," Phys. Rev. B **76**(24), 245327 (2007).
[6]A. Khoshaman, H. D. E. Fan, A. Koch, G. Sawatzky, and A. Nojeh, "Thermionics, thermoelectrics, and nanotechnology: New possibilities for old ideas," IEEE Nanotechnol. Mag. **8**(2), 4–15 (2014).
[7]G. N. Hatsopoulos and E. P. Gyftopoulos, *Thermionic Energy Conversion* (MIT Press, 1973), Vol. 1.
[8]N. S. Rasor, "Thermionic energy conversion plasmas," IEEE Trans. Plasma Sci. **19**(6), 1191–1208 (1991).
[9]G. N. Hatsopoulos and E. P. Gyftopoulos, *Thermionic Energy Conversion - Vol. 2: Theory, Technology, and Application* (MIT Press, 1979).
[10]*CRC Handbook of Chemistry and Physics*, 93rd ed., edited by W. M. Haynes (CRC Press, 2012).
[11]J. A. Bittencourt, *Fundamentals of Plasma Physics* (Springer, New York, 2004).
[12]P. L. Auer, "Potential distributions in a low-pressure thermionic converter," J. Appl. Phys. **31**(12), 2096–2103 (1960).
[13]R. G. McIntyre, "Extended space-charge theory in low-pressure thermionic converters," J. Appl. Phys. **33**(8), 2485–2489 (1962).
[14]A. H. Khoshaman and A. Nojeh, "Classical momentum gap for electron transport in vacuum and consequences for space charge in thermionic converters with a grid electrode," J. Vac. Sci. Technol. B **34**(4), 40610 (2016).
[15]A. H. Khoshaman and A. Nojeh, "A self-consistent approach to the analysis of thermionic devices," J. Appl. Phys. **119**(4), 44902 (2016).
[16]A. H. Khoshaman, A. T. Koch, M. Chang, H. D. E. Fan, M. V. Moghaddam, and A. Nojeh, "Nanostructured thermionics for conversion of light to electricity: Simultaneous extraction of device parameters," IEEE Trans. Nanotechnol. **14**(4), 624–632 (2015).
[17]A. H. Khoshaman, M. Chang, and A. Nojeh, "Extraction of multiple parameters of a light-activated thermionic cathode with a single type of experiment," in *26th International Vacuum Nanoelectronics Conference (IVNC)* (2013), pp. 1–2.
[18]A. H. Khoshaman and A. Nojeh, "A comprehensive approach to the analysis of nano-thermionic convertors through particle tracing," in *28th International Vacuum Nanoelectronics Conference (IVNC)* (2015), pp. 36–37.